Matter

CellPress

Article

Dynamically modulated gating process of nanoporous membrane at sub-2-nm speed

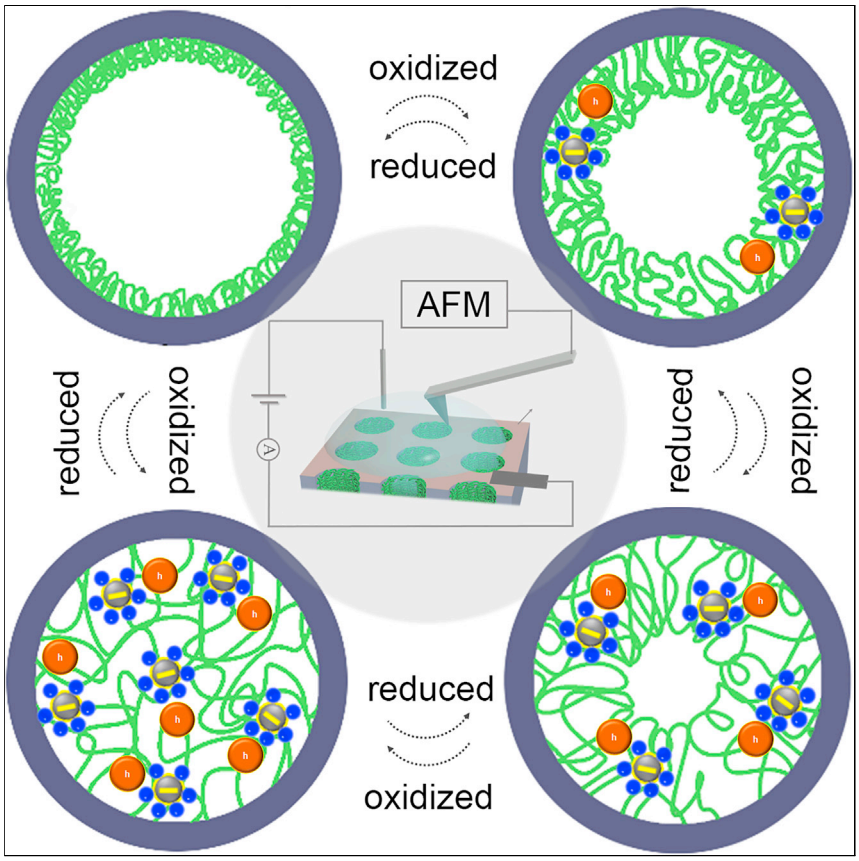

We precisely modulate the dynamic electric gating process in a polypyrrole (PPy)-based nanoporous membrane system at sub-2-nm speed. The thickness of the polymer film in nanochannels changes by 83%. The successive polymer chain variation at nanoscale is observed by atomic force microscope (AFM) *in situ*. The small operation voltage (−0.5 to 0.8 V) and quantitative variation, along with biocompatible materials, make this membrane promising for smart wearable applications. Our membrane strategy also provides some inspiration toward advanced separation membrane on nanoscale.

Demonstrate
Proof-of-concept of performance with intended application/response

Yahong Zhou, Junran Hao, Jiajia Zhou, ..., Chengyun Ning, Xuliang Deng, Lei Jiang

zhouyh@mail.ipc.ac.cn (Y.Z.)
imcyning@scut.edu.cn (C.N.)
kqdengxuliang@bjmu.edu.cn (X.D.)

Highlights

We modulate the dynamic electric gating process in nanoporous membrane at sub-2-nm speed

The thickness of the polymer film in nanochannels changes by 83%

The successive polymer chain variation at nanoscale is observed by AFM *in situ*

Zhou et al., Matter 5, 281–290
January 5, 2022 © 2021 Elsevier Inc.
https://doi.org/10.1016/j.matt.2021.11.024

Matter

CellPress

Article

Dynamically modulated gating process of nanoporous membrane at sub-2-nm speed

Yahong Zhou,[1,2,6,8,9,*] Junran Hao,[1,8] Jiajia Zhou,[2,7,8] Jingwen Liao,[2,4,8] Yan Wei,[3,8] Xiachao Chen,[5] Chengyun Ning,[2,*] Xuliang Deng,[3,*] and Lei Jiang[1,6]

SUMMARY

Gating properties of nanochannels, as the key nanofluidic behavior, have huge applications in sensing, mass transportation, and separation. The terminal "open" and "closed" states in response to changes in environments have been widely studied. Yet to date, control of the dynamic gating process at quantitatively nanoscale speed remains a great challenge. Here, we modulate the dynamically electric gating process in a polypyrrole (PPy)-based nanoporous membrane system at sub-2-nm speed. The nanoconfinement environment endows the polymer chain with excellent electrochemical properties, and the polymer film swells or contracts at a controlled speed, accompanied by a reversible counterion uptake or expulsion. With this switching process, the thickness of the polymer changes by 83%, resulting in a fully closed gating state. In addition to atomic force microscope (AFM) topography *in situ*, the small operation voltages and ultra-high-strain scope, along with biocompatible materials, make this design promising for smart nanorobot and wearable electronics.

INTRODUCTION

Biological channels embedded in cell membranes can precisely control mass transport, usually by fine-tuning dwelling time at the membrane.[1,2] Inspired by this gating property, researchers have created an abundance of smart nanoporous membranes for their huge applications in biosensing, liquid and chemical separation, drug delivery, energy conversion, etc.[3–7] The rational design of a gating nanoporous membrane aims to modify the surface chemistry of the channels in response to external stimuli[8–12] or build channels with a tunable shape.[13] Recently, the dynamic gating process has also been investigated in microporous membranes, wettability-tunable membranes, and gas-transport membranes.[14–16] Among these gating membranes, controlling pore size is a key factor, which plays a vital role in permeability and selectivity.[17,18] The ability of *in situ* precise size modulation is critical for nanofluidic devices, which benefit the high-precision separation and single-species selectivity. However, the exquisite tuning of the radius of the nanochannels still remains a challenge, especially at a quantitatively nanoscale speed.

Generally, polymer brushes are widely adapted to modify the surface chemistry of the pore, and the reversible chemical configuration switch renders the membrane able to respond to pH, temperature, ions, magnetic or electric fields, etc.[19–21] Similar to liquid, polymer brushes may behave quite differently in a nanoconfined environment. Exploring the interplay of polymer brushes with ions in a confined environment remains elusive but important; for example, polymer expansion in a battery

Progress and potential

Gating properties of nanochannels, as a key nanofluidic behavior, have huge applications in sensing, mass transportation, and separation. Yet to date, control of the dynamic gating process at quantitatively nanoscale speed remains a great challenge. Here, we precisely modulate the dynamic electric gating process in a polypyrrole (PPy)-based nanoporous membrane system at sub-2-nm speed. The nanoconfinement environment endows the PPy-based nanoporous membrane with excellent electrochemical properties. Thus, this platform provides a small operation voltage (−0.5 to 0.8 V) for directly observing the successive polymer chain variation at nanoscale (ca. 10 nm) by atomic force microscope topography *in situ*. Furthermore, the thickness of the polymer changes by 83%, resulting in a fully closed gating state, which has not been reported so far. This small operation voltage, along with ultra-high-strain scope, makes this membrane promising for smart nanorobot and bioactuator applications.

largely decreases the lifespan of the battery.[22] Therefore, exploring the polymer volume expansion and contraction mechanism is critical for polymer application. Conducting polymers, with surface charge and volume variation along the redox process, have been extensively studied in smart nanopores, mainly based on the electric inducing gating and rectifying current.[23–28] In these works, the two terminated states (i.e., the fully reduced and oxidized states) are intensely studied. However, the dynamics of the swelling process has long been underestimated, especially from a quantitative aspect.[29–32]

RESULT AND DISCUSSION

Here, we modulate the dynamically electric gating process in a polypyrrole (PPy)-based nanoporous membrane system at sub-2-nm speed. By modifying PPy onto an anodic aluminum oxide (AAO) membrane, a series of conducting polymer nanoporous membranes (CPNMs) were obtained (Figures S1 and S2). Owing to the nanoconfined environment, the intrapore PPy is associated with chain-like polymer growth and lower electrical resistance.[31,33,34] Thus, with a small operating window (−0.5 to 0.8 V), PPy film contracts or swells at a controlled speed accompanied by a reversible counterion uptake or expulsion. Then, a successive polymer chain variation process is directly observed at nanoscale (ca. 10 nm) by atomic force microscope (AFM) topography *in situ*. In addition, through this, we observed the polymer brush expansion and contraction behavior of exchanging ions with the electrolyte when applied with a bias. As shown in Figure 1A by testing the ionic transmembrane property with electric stimuli *in situ*, a redox voltage gating nanofluidic device was successfully constructed, confirmed by transmission electron microscopy (TEM) images (Figure 1B). The largest inner diameter (39.8 nm) of CPNMs (labeled as "switch-on state") and the smallest diameter (i.e., nearly 0 nm of inner diameter) CPNMs (labeled as "switch-off state") were obtained. The channels are fully blocked by the polymer film eventually, which has not been reported so far. With this switching process, the thickness of the polymer changes by 83%, while the volume expands almost three times. In addition to the two terminated states, a successive spatial change along the radial direction was observed, resulting in a regulated pore size (Figures 1C and 1D) and controlled ionic transmembrane conductance. Through AFM *in situ*, nanometer-scale expansion and contraction of the polymer chain were directly observed.

Modulated ionic transmembrane conductance at controlled speed

In the nanofluidic system, both the surface charge and the pore size benefit the ionic transport conductance. The contribution of surface charge to conductivity is mainly dominated by the salt concentration, which affects the thickness of the electric double layer.[4,35] Here, to directly verify that the radius variation in our system dominated the transmembrane conductance, we tested the dependence of the conductance on the ionic concentration. While in dilute salt solution (0.01 M KCl), the current-voltage curve is nonlinear, and the membrane shows ionic current rectification (Figure 2A). However, with increasing ionic concentration, the linear current-versus-voltage curve appears (Figure 2B). Our experimental data demonstrated that the ions travel across the membrane linearly in 0.1 M KCl solution. In this case, the impact of surface charge on the conductivity could be neglected, because the surface charge is screened by the concentrated counterions and the Debye length is very small (estimated to be 0.95 nm). On the other hand, the charges on the polymer brush increase if the membrane is applied with an oxidation potential. If the contribution of the surface charge works, here, the conductance is supposed to deviate from the bulk. In our system, this trend is the opposite, and the tested current continues to decline.

[1]CAS Key Laboratory of Bio-inspired Materials and Interfacial Science, Technical Institute of Physics and Chemistry, Chinese Academy of Sciences, Beijing 100190, PR China

[2]School of Molecular Science and Engineering, South China University of Technology, Guangzhou 510640, PR China

[3]Department of Geriatric Dentistry, Peking University School and Hospital of Stomatology, Beijing 100081, PR China

[4]Frontier Science and Technology Research Center, Guangzhou Institute of Advanced Technology, Guangzhou 511458, PR China

[5]School of Materials Science and Engineering, Zhejiang Sci-Tech University, Hangzhou 310018, PR China

[6]School of Chemistry, Beihang University, Beijing, PR China

[7]South China Advanced Institute for Soft Matter Science and Technology, Guangdong Provincial Key Laboratory of Functional and Intelligent Hybrid Materials and Devices, South China University of Technology, Guangzhou 510640, PR China

[8]These authors contributed equally

[9]Lead contact

*Correspondence: zhouyh@mail.ipc.ac.cn (Y.Z.), imcyning@scut.edu.cn (C.N.), kqdengxuliang@bjmu.edu.cn (X.D.)

https://doi.org/10.1016/j.matt.2021.11.024

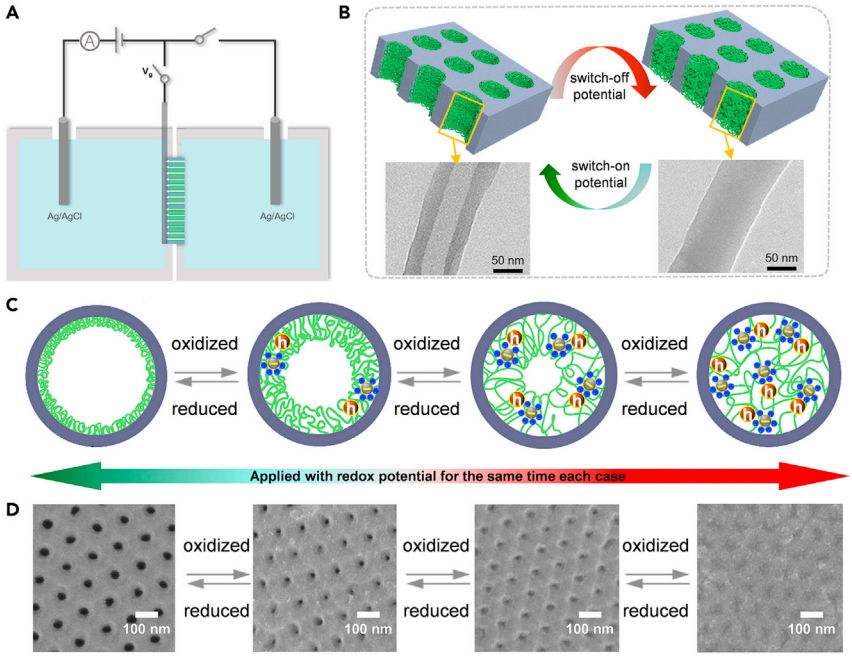

Figure 1. Dynamic electric gating in a conducting polymer integrated porous membrane system

(A) Electrical measurements of the nanoporous membrane.

(B) Schematic of the gating property of the membrane (top) and the process shown by TEM images (bottom). The full open and closed states of the CPNMs correspond to the oxidative and reduced states, respectively.

(C) Schematic of speed-controlled channel radius with redox process.

(D) Radius of CPNM varies with time of redox potential across the membrane.

This result reveals that the spatial volume dominates the current in these pores. As a first-order approximation, the nanoporous membrane with polypyrrole film could be considered as cylindrical pores. The conductance is mainly determined by the diameter of the pores (Figure S5): $G = \kappa_b * \pi d^2/4L$, where κ_b is the bulk conductivity and L and d are the length and diameter of the nanopore, respectively. In our CPNM system, the conductance is proportional to the diameter of the channel. All the data reported next in this article were detected in 0.1 M KCl, where the surface charge effect could be neglected (where the Debye length is ca. 0.95 nm, which is far less than the diameter of the pore).

Owing to the excellent electrochemical property of the membrane (Figure S7), the transmembrane conductance exhibited a periodic switch between nearly 0 and approximately 90 μs, if the membrane was applied at a periodic potential stimulus for 10 min (insets in Figure 2C are SEM images of the corresponding CPNMs in the periodic open and closed states, Figures S8–S10). Through this gating process, the current dropped nearly three to four orders of magnitude. Particularly, through periodic switching potentials for 100 cycles, ionic conductance remained relatively stable, demonstrating the robustness of our CPNMs (Figure S11).

To explore the situation where the membrane is partially charged, we tested the transmembrane conductance by applying different times of bias. We performed a series of experiments for investigating the dynamic current change via time in response to electric field. This phenomenon was observed with the potentiostatic mode. As shown in the device diagram in Figure 1A, a bias of 0.5 V was directly

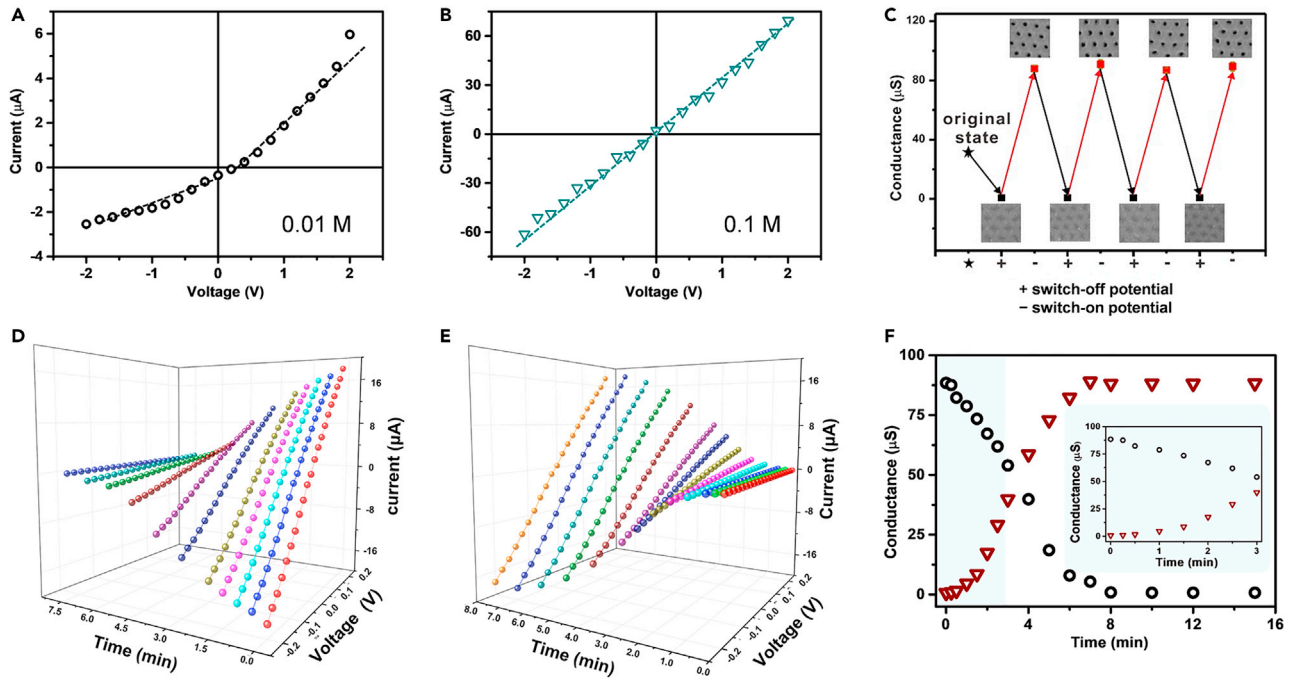

Figure 2. Electrical and ionic conducting properties of the CPNM

(A and B) Ionic current across the membrane in different electrolyte concentrations (A, 0.01 M; B, 0.1 M).

(C) Reversible switch in ion transport achieved by applying periodic switching potentials for 10 min. Each point is the average of five experiments. Insets are SEM images of CPNM in periodic open (switch-on) and closed (switch-off) states.

(D and E) Ionic current varies with application time of *in situ* switch-on a and switch-off b potentials (D, 500 mV; E, −800 mV).

(F) The conductance varies as a function of time while the membrane is applied with redox potential. The inset image is the conductance variation in the first 3 min. All data in (C–F) were obtained from CPNMs that were fabricated by 10 cycles of cyclic voltammetry as well. The conductance measurement was performed in 0.1 M KCl.

applied onto the polymer brush for 15 s. The current slightly dropped as shown in Figure 2D. After several runs, the current continued to decrease until the value of the current had fallen to almost zero. At this stage, the channels stayed closed, even though bias was still applied across the membrane. In contrast, the current would rise if a reduction potential (−0.8 V) was applied. Clearly, the current increased steadily until it reached the maximum value as shown in Figure 2E. If the membrane was completely reduced, the current remained at this peak. Figure 2F demonstrates that the transmembrane conductance decreases or increases continuously with an applied bias. When it drops to zero or rises to the maximum value, the conductance will not change, corresponding to the complete oxidation or reduction state of the conducting polymer. These two processes are reversible and completely opposite. Based on the equation between the radius and the conductance, and the minimum and maximum value of the conductance corresponding to the terminated states of the closed and open states, we estimated that the pore size could be tuned precisely every 1.5 nm each time (by applying a potential for 15 s). Although numerous materials have been explored to prepare solid nanopores, it remains a great challenge to precisely modulate it under 10 nm, not even tuning the pore size for an as-prepared pore, especially for the soft matter.[27,32,33]

In situ AFM topography variation as a function of time with an applied bias

As discussed above, to study the effect of polymer expansion and contraction on transmembrane conductance, we chose a relatively high ionic concentration to test where the contribution of surface charge is shielded. We also tested the spatial

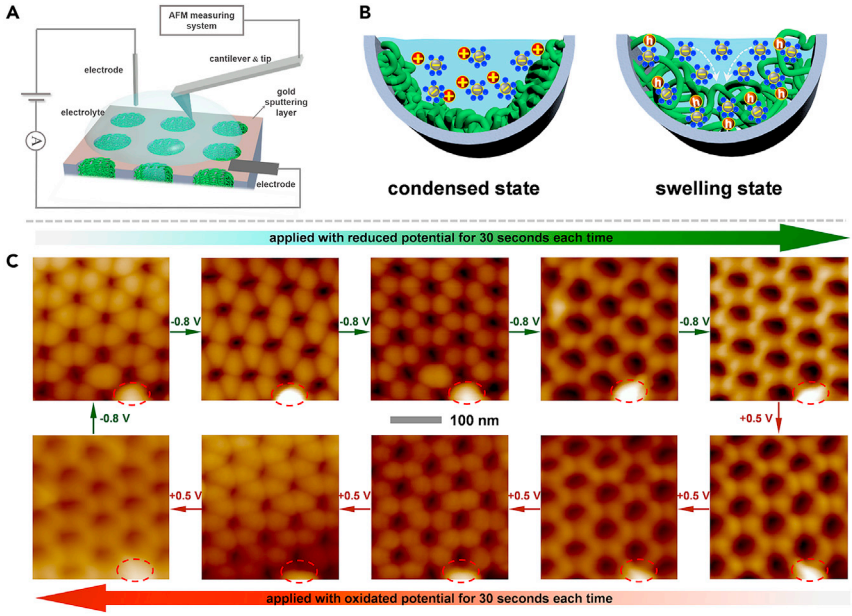

Figure 3. *In situ* AFM imaging as a function of the electric field effect

(A) The setup of the AFM measurement with electric field.

(B) Schematics of different polymer brush modes in the AFM experiment, with the ions expelled outward or penetrating into the polymer film.

(C) Topography of the polymer film varies as a function of time with the applied bias, and this process is reversible. All the data were measured in 100 mM KCl electrolytes. Red circles marked in (C) show the same spot during the AFM experiment.

change with redox potential in 100 mM KCl by AFM *in situ* (Figure 3A). By probing the horizontal displacement of the polymer brush confined in the nanopores, we directly observed the polymer film variation process under electric field. As shown in Figure 3B, the morphology of the polymer in a confined environment changes in accordance with the ion takeup in the electrolyte.[22,36] The radius in the original state was 11.2 $\pm$ 2.2 nm. It increased to 19.1 $\pm$ 2.1 nm when a bias of -0.8 V was applied to the membrane for 30 s so that the doping ions drifted out of the polymer brush. After several runs, the polymer film contracted to the fully opened state with a radius of 49.8 $\pm$ 4.7 nm. Under an oxidizing bias, the polymer film swelled subsequently and finally completely blocked the pore. The polymer chain in the nanoconfinement environment exhibits a unique performance.[37] With this switching process, the thickness of the polymer changes by 83%, which is much higher than previous reports.[14,38] Owing to the excellent electrochemical property of PPy in such a nanoconfined environment, this process is reversible. Hence, we directly observed that the reversible expansion and contraction scope depend on the input charge along the polymer chain (Figure 3B). These data are in accord with data regarding modulation in ionic transmembrane current during continuous electric regulation.

Adjusting ionic transmembrane conductance at tunable speed

We noticed that the volume swelling and contraction scale may be correlated to the amount of charge along the polymer chain. The number of electric charges stored in the membrane could be tuned with the applied voltage or current. As shown in Figure 4A, the polymer brushes were charged or discharged with different amounts of electrons or holes through the galvanotactic method. Then the tested ionic transmembrane conductance was continuously adjustable in a wide range. From the initial state to the full oxidation and then back to the initial state, we realized the

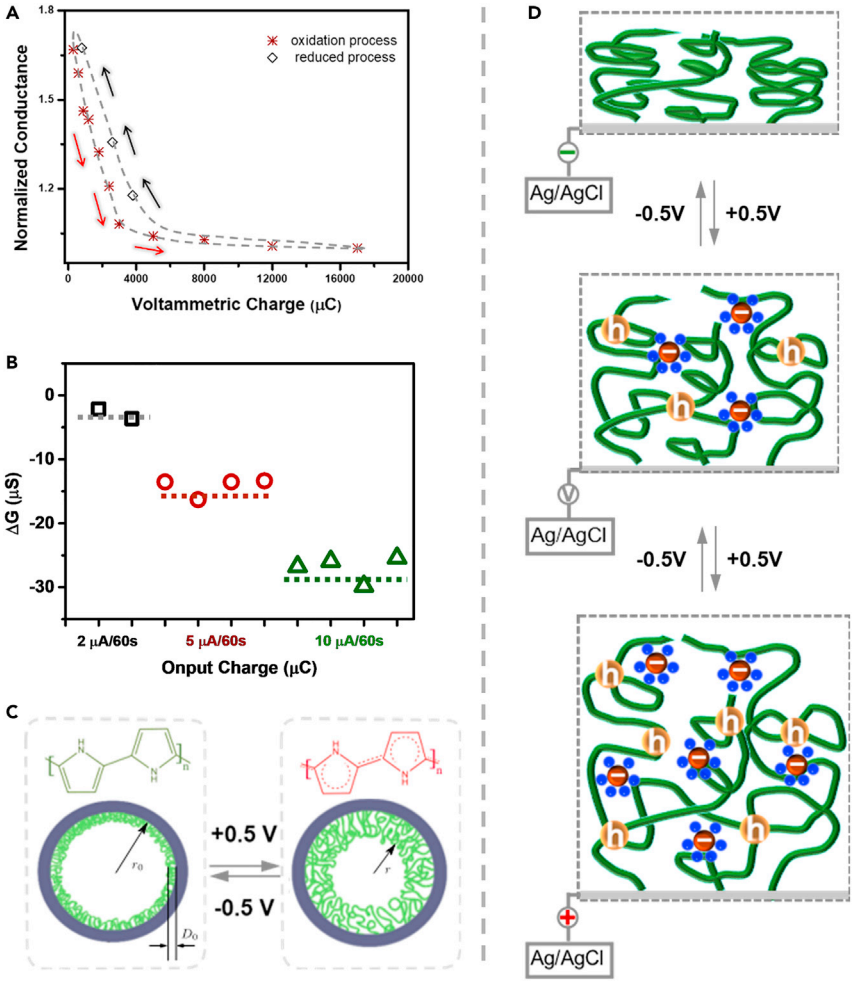

Figure 4. Volume expansion and contraction mechanism as a function of the input charge onto the polymer brushes

(A) Conductance varies as a function of the voltammetric charge with modulated speed. The data were collected in the CPNM with thinner polymer brushes; thus, the conductance of the oxidized state did not reach zero (Figure S3).

(B) The change in transmembrane conductance depends on the input charge onto the polymer every 1 min.

(C) The reversal chemical configuration switch, induced by electric field, corresponds to the volume contraction and expansion states of the polymer film.

(D) The swelling mechanism depending on the number of positive holes along the polymer (equilibrium between the solvated ions from the electrolyte and the positive holes along the polymer chain).

closed-loop adjustment with variable rates. At the beginning, four stimuli (current density 5 μA for 60 s) were applied consecutively to the membrane, the transmembrane conductance dropped continuously, and the change in conductance was basically maintained at a stable level. Then, a current density of 10 μA/cm^2 every minute was charged onto the membrane, and the conductance continued to decrease at a higher speed. On the third stimulus, the conductance changed slowly. Then current densities of 15, 20, and 25 μA for 1 min were applied to the membrane, and the conductance did not show a significant increase, as it could not be oxidized further. During this period, the membrane underwent an oxidation reaction. Then, a current density of 20 μA was applied on the membrane for 1 min. Clearly, the conductance

increased sharply, and this trend was the same for another stimulus (20 μA/cm^2 for 1 min). Finally, a larger stimulus (30 μA for 1 min) was added onto the membrane, and the conductance returned to the same value as the initial state. The entire circle was completed in this redox process at variable speed. This showed that the expansion rate of the polymer could be regulated by the amount of electricity given per unit time. It revealed that the volume swelling speed of the polymer brush could be precisely modulated by controlling the total amount of input charge per unit time. With the applied current increased, the transmembrane conductance began to change, and the amplitude of change increased with the increased input current density. Instant overoxidation or overreduction may have occurred if excessive current were applied. In addition, this gating process was suitable for various electrolyte solutions (Figure S14) and temperature conditions (Figure S15) and had the best performance under acidic aqueous solutions (Figure S16).

Mechanism of volume expansion and contraction during charging and discharging

The interplay between the electrolyte and the semiconducting network gives plenty of room to explore. The swelling equilibrium of the polymer network is the result of a balance between two competing processes.[39–41] The polymer brush moves freely along the radical direction of the pore while other directions are limited.

(1) Elastic pressure:

When the polymer network is expanded from its native state, there is an elastic restoring force, which resists the expansion. The elastic contribution can be written as an elastic pressure, given by

$$\frac{\Pi_{el}}{k_B T} = A\frac{\varphi}{N}\frac{R^2}{R_0^2}, \qquad \text{(Equation 1)}$$

where φ is the polymer concentration and N is the number of statistical units of a strand. The combination of $A\varphi/N$ gives the number density of the strands. These strands act like elastic strings, and the averaged end-to-end distances in the reference state (without swelling) and the swollen state are R_0^2 and R^2, respectively. For the Gaussian chain model, $R_0^2 = Nb^2$, where b is the statistical unit length (Kuhn length). The prefactor A in Equation 1 depends on the network model.

(2) Osmotic pressure:

On the other hand, the driving force to expand the network is from the osmotic pressure Π_{os}. For networks composed of charged chains and under low salt concentration, the osmotic pressure is essentially the result of counterion's entropy,[42]

$$\frac{\Pi_{os}}{k_B T} = \left[1 - \frac{l_B}{2\Lambda}\right]\alpha\varphi \qquad \text{(Equation 2)}$$

where α is the fraction of charged monomer in the network, $l_B = e^2/(4\pi\varepsilon k_B T)$ is the Bjerrum length, and $\Lambda = b/\alpha$ is the contour length between two consecutive charges. In the limit of Manning condensation, strongly charged chains are screened, and the effective charge of the polyelectrolyte chain is renormalized, leading to $\Lambda = l_B$. Equation 2 is then simplified to

$$\frac{\Pi_{os}}{k_B T} = \frac{1}{2}\alpha\varphi. \qquad \text{(Equation 3)}$$

The balance between elastic pressure (1) and osmotic pressure (2) gives

$$\frac{R}{R_0} \sim N^{1/2}\alpha^{1/2} \Rightarrow R \sim Nb\alpha^{1/2}. \quad \text{(Equation 4)}$$

If the polymer network is confined in nanopores, the gel could expand or contract in the radical direction. In this case, the area of the cross section is swollen according to Equation 4:

$$\frac{\pi\left(r_0^2 - r^2\right)}{2\pi r_0 D_0} \sim \alpha^{1/2}. \quad \text{(Equation 5)}$$

So the radius of CPNMs swells or contracts with the charging or discharging process (redox process) along the backbone. Here, r is the radius of the conducting polymer porous membrane, r_0 is the original radius, and D_0 is the original thickness of the polymer gel. This relationship accurately predicts that, confined in the nanochannels, the radius of the membrane could be modulated by regulating the charges along the conducting polymer. So this rationale could be used to design dynamic gating transport in nanochannels by varying the diameters at controlled speed at nanometer scale.

DISCUSSION

Previously, conducting polymer film as soft actuator matter was widely used. However, the nature of the polymer chain movement induced by doping ions is unique to organic semiconductors, yet poorly understood. The nanoconfinement environment endows the PPy-based nanoporous membrane with excellent electrochemical properties. Thus, this platform provides a small operation voltage (−0.5 to 0.8 V) for directly observing the successive polymer chain variation at nanoscale (ca. 10 nm) by AFM topography *in situ*. Furthermore, the thickness of the polymer changes by 83%, resulting in a fully closed gating state, which has not been reported before. Here, we also set up a model to study the polymer brush behavior in an extremely nanoconfined environment. The polymer film exhibits contraction and swelling at quantitative speed by certain charged electrons or holes along the conducting polymer brush. The remarkable volume change of PPy in such a confined environment makes this kind of material promising for nanobots as well. The small operation voltages (−0.5 to 0.8 V) and quantitative variation, along with biocompatible materials, make this membrane promising for smart wearable applications. Our membrane strategy also provides some inspiration toward advanced separation membranes on the nanoscale.

EXPERIMENTAL PROCEDURES

Resource availability

Lead contact

Further information and requests for resources and reagents should be directed to and will be fulfilled by the lead contact, Yahong Zhou (zhouyh@mail.ipc.ac.cn).

Materials availability

This study did not generate new unique reagents.

Data and code availability

This study did not generate or analyze datasets or code.

Nanoporous membrane fabrication

The detailed synthetic steps are described in the supplemental information. CPNMs were embedded in AAO membranes by electrochemical polymerization, during which the PPy was gradually electropolymerized onto the inner wall of the AAO

membrane. By adjusting the polymerization time, we obtained a series of CPNMs with inner diameters ranging from 0 to 96.2 nm (Figures S1–S6).

AFM topography test with electric stimuli

All AFM experiments were performed with a Bruker Dimension ICON SPM in ScanAsyst-fluid mode (Bruker, Germany). A copper foil, which is the electrode of the Keithley 6487 picometer, was attached to the membranes with silver conducting paste. The membranes were immersed in 0.1 M KCl solution during the test process.

Ionic transmembrane record

The nanofluidic property of the CPNMs was tested by measuring the ionic current through the membrane with a redox potential. The current was recorded by a Keithley 6487 picometer (Keithley Instruments, Cleveland, OH). The membrane was mounted within a two-compartment electrochemical cell as shown in Figure 1A. Ag/AgCl electrodes were used to apply a transmembrane potential, and a copper foil was used to apply potential as an electric stimulus.

SUPPLEMENTAL INFORMATION

Supplemental information can be found online at https://doi.org/10.1016/j.matt.2021.11.024.

ACKNOWLEDGMENTS

We appreciated the technical support from Peking University School and Hospital of Stomatology. We thank the Fantastic Color Co., Ltd. (Beijing, China), for graphic design assistance. This work was funded by National Science Foundation of China grants 21875270, 21774004, 21988102, and 51703037; Youth Innovation Promotion Association of the Chinese Academy of Sciences grant 2021029; and Guangzhou Science and Technology Program grant 202102080633.

AUTHOR CONTRIBUTIONS

Y.Z., X.D., C.N., and L.J. conceived the idea. J.L. and J.H. performed the experiments. Y.Z. and J.Z. analyzed and interpreted the results. Y.Z. drafted the manuscript, and all authors contributed to the writing of the manuscript.

DECLARATION OF INTERESTS

The authors declare no competing interests.

Received: August 19, 2021
Revised: October 31, 2021
Accepted: November 24, 2021
Published: December 15, 2021

REFERENCES

1. Case, L.B., Zhang, X., Ditlev, J.A., and Rosen, M.K. (2019). Stoichiometry controls activity of phase-separated clusters of actin signaling proteins. Science *363*, 1093–1097.
2. Sheng, Z., Zhang, J., Liu, J., Zhang, Y., Chen, X., and Hou, X. (2020). Liquid-based porous membranes. Chem. Soc. Rev. *49*, 7907–7928.
3. Hummer, G., Rasaiah, J.C., and Noworyta, J.P. (2001). Water conduction through the hydrophobic channel of a carbon nanotube. Nature *414*, 188–190.
4. Sparreboom, W., van den Berg, A., and Eijkel, J.C.T. (2009). Principles and applications of nanofluidic transport. Nat. Nanotechnol. *4*, 713–720.
5. Siwy, Z.S., and Howorka, S. (2010). Engineered voltage-responsive nanopores. Chem. Soc. Rev. *39*, 1115–1132.
6. Hou, X., Hu, Y., Grinthal, A., Khan, M., and Aizenberg, J. (2015). Liquid-based gating mechanism with tunable multiphase selectivity and antifouling behaviour. Nature *519*, 70–73.
7. Hou, Y., and Hou, X. (2021). Bioinspired nanofluidic iontronics. Science *373*, 628–629.
8. Di Fiori, N., Squires, A., Bar, D., Gilboa, T., Moustakas, T.D., and Meller, A. (2013). Optoelectronic control of surface charge and translocation dynamics in solid-state nanopores. Nat. Nanotechnol. *8*, 946–951.
9. Keyser, U.F. (2011). Controlling molecular transport through nanopores. J. R. Soc. Interfaces *8*, 1369–1378.

10. Branton, D., Deamer, D.W., Marziali, A., Bayley, H., Benner, S.A., Butler, T., Di Ventra, M., Garaj, S., Hibbs, A., Huang, X., et al. (2008). The potential and challenges of nanopore sequencing. Nat. Biotech. *26*, 1146–1153.

11. Yusko, E.C., Johnson, J.M., Majd, S., Prangkio, P., Rollings, R.C., Li, J., Yang, J., and Mayer, M. (2011). Controlling protein translocation through nanopores with bio-inspired fluid walls. Nat. Nanotechnol. *6*, 253–260.

12. Zhu, X., Zhou, Y., Hao, J., Bao, B., Bian, X., Jiang, X., Pang, J., Zhang, H., Jiang, Z., and Jiang, L. (2017). A charge-density-tunable three/two-dimensional polymer/graphene oxide heterogeneous nanoporous membrane for ion transport. ACS Nano *11*, 10816–10824.

13. Wang, M., Meng, H., Wang, D., Yin, Y., Stroeve, P., Zhang, Y., Sheng, Z., Chen, B., Zhan, K., and Hou, X. (2019). Dynamic curvature nanochannel-based membrane with anomalous ionic transport behaviors and reversible rectification switch. Adv. Mater. *31*, 1805130.

14. Tan, X., Hu, C., Zhu, Z., Liu, H., and Qu, J. (2019). Electrically pore-size-tunable polypyrrole membrane for antifouling and selective separation. Adv. Funct. Mater. *29*, 1903081.

15. Mi, L., Yu, J., He, F., Jiang, L., Wu, Y., Yang, L., Han, X., Li, Y., Liu, A., Wei, W., et al. (2017). Boosting gas involved reactions at nanochannel reactor with joint gas–solid–liquid interfaces and controlled wettability. J. Am. Chem. Soc. *139*, 10441–10446.

16. Liu, Y., Chow, C.-M., Phillips, K.R., Wang, M., Voskian, S., and Hatton, T.A. (2020). Electrochemically mediated gating membrane with dynamically controllable gas transport. Sci. Adv. *6*, eabc1741.

17. Epsztein, R., DuChanois, R.M., Ritt, C.L., Noy, A., and Elimelech, M. (2020). Towards single-species selectivity of membranes with subnanometre pores. Nat. Nanotechnol. *15*, 426–436.

18. Liu, Z., Wang, W., Xie, R., Ju, X.-J., and Chu, L.-Y. (2016). Stimuli-responsive smart gating membranes. Chem. Soc. Rev. *45*, 460–475.

19. Wang, S., Zhang, Y., Han, Y., Hou, Y., Fan, Y., and Hou, X. (2021). Design of porous membranes by liquid gating technology. Acc. Mater. Res. *2*, 407–419.

20. Sheng, Z., Zhang, M., Liu, J., Malgaretti, P., Li, J., Wang, S., Lv, W., Zhang, R., Fan, Y., Zhang, Y., Chen, X., and Hou, X. (2020). Reconfiguring confined magnetic colloids with tunable fluid transport behavior. Natl. Sci. Rev. *8*, nwaa301.

21. Eygeris, Y., White, E.V., Wang, Q., Carpenter, J.E., Grunwald, M., and Zharov, I. (2019). Responsive nanoporous membranes with size selectivity and charge rejection from self-assembly of polyelectrolyte "hairy" nanoparticles. ACS Appl. Mater. Interfaces *11*, 3407–3416.

22. Giridharagopal, R., Flagg, L.Q., Harrison, J.S., Ziffer, M.E., Onorato, J., Luscombe, C.K., and Ginger, D.S. (2017). Electrochemical strain microscopy probes morphology-induced variations in ion uptake and performance in organic electrochemical transistors. Nat. Mater. *16*, 737.

23. Bao, B., Hao, J., Bian, X., Zhu, X., Xiao, K., Liao, J., Zhou, J., Zhou, Y., and Jiang, L. (2017). 3D porous hydrogel/conducting polymer heterogeneous membranes with electro-/pH-modulated ionic rectification. Adv. Mater. *29*, 1702926.

24. Pérez-Mitta, G., Marmisollé, W.A., Trautmann, C., Toimil-Molares, M.E., and Azzaroni, O. (2017). An all-plastic field-effect nanofluidic diode gated by a conducting polymer layer. Adv. Mater. *29*, 1700972.

25. Perez-Mitta, G., Marmisolle, W.A., Trautmann, C., Toimil-Molares, M.E., and Azzaroni, O. (2015). Nanofluidic diodes with dynamic rectification properties stemming from reversible electrochemical conversions in conducting polymers. J. Am. Chem. Soc. *137*, 15382–15385.

26. Zhang, Q., Liu, Z., Wang, K., and Zhai, J. (2015). Organic/inorganic hybrid nanochannels based on Polypyrrole-embedded alumina nanopore arrays: pH- and light-modulated ion transport. Adv. Funct. Mater. *25*, 2091–2098.

27. Laucirica, G., Toimil-Molares, M.E., Trautmann, C., Marmisollé, W., and Azzaroni, O. (2020). Polyaniline for improved blue energy Harvesting: highly rectifying nanofluidic diodes operating in hypersaline conditions via one-step functionalization. ACS Appl. Mater. Interfaces *12*, 28148–28157.

28. Hery, T., and Sundaresan, V.-B. (2016). Ionic redox transistor from pore-spanning PPy(DBS) membranes. Energy Environ. Sci. *9*, 2555–2562.

29. Lizarraga, L., Maria Andrade, E., and Victor Molina, F. (2004). Swelling and volume changes of polyaniline upon redox switching. J. Electroanal. Chem. *561*, 127–135.

30. Chen, X., Xing, K.-Z., and Inganäs, O. (1996). Electrochemically induced volume changes in poly(3,4-ethylenedioxythiophene). Chem. Mater. *8*, 2439–2443.

31. Brinker, M., Dittrich, G., Richert, C., Lakner, P., Krekeler, T., Keller, T.F., Huber, N., and Huber, P. (2020). Giant electrochemical actuation in a nanoporous silicon-polypyrrole hybrid material. Sci. Adv. *6*, eaba1483.

32. Angevine, C.E., Robertson, J.W.F., Dass, A., and Reiner, J.E. (2021). Laser-based temperature control to study the roles of entropy and enthalpy in polymer-nanopore interactions. Sci. Adv. *7*, eabf5462.

33. Schultze, J.W., and Jung, K.G. (1995). Regular nanostructured systems formed electrochemically: deposition of electroactive polybithiophene into porous silicon. Electrochim. Acta *40*, 1369–1383.

34. Zhang, Q., Zhang, Z., Zhou, H., Xie, Z., Wen, L., Liu, Z., Zhai, J., and Diao, X. (2017). Redox switch of ionic transport in conductive polypyrrole-engineered unipolar nanofluidic diodes. Nano Res. *10*, 3715–3725.

35. Lee, C., Joly, L., Siria, A., Biance, A.-L., Fulcrand, R., and Bocquet, L. (2012). Large apparent electric size of solid-state nanopores due to spatially extended surface conduction. Nano Lett. *12*, 4037–4044.

36. Bay, L., West, K., Sommer-Larsen, P., Skaarup, S., and Benslimane, M. (2003). A conducting polymer artificial muscle with 12%linear strain. Adv. Mater. *15*, 310–313.

37. Smela, E., and Gadegaard, N. (2001). Volume change in polypyrrole studied by atomic force microscopy. J. Phys. Chem. B *105*, 9395–9405.

38. Suárez, M.F., and Compton, R.G. (1999). In situ atomic force microscopy study of polypyrrole synthesis and the volume changes induced by oxidation and reduction of the polymer. J. Electroanal. Chem. *462*, 211–221.

39. Skouri, R., Schosseler, F., Munch, J.P., and Candau, S.J. (1995). Swelling and elastic properties of polyelectrolyte gels. Macromolecules *28*, 197–210.

40. Csajka, F.S., Netz, R.R., Seidel, C., and Joanny, J.F. (2001). Collapse of polyelectrolyte brushes: scaling theory and simulations. Eur. Phys. J. E *4*, 505–513.

41. Das, S., Banik, M., Chen, G., Sinha, S., and Mukherjee, R. (2015). Polyelectrolyte brushes: theory, modelling, synthesis and applications. Soft Matter *11*, 8550–8583.

42. Joanny, J.F., and Pincus, P. (1980). Electrolyte and polyelectrolyte solutions: limitations of scaling laws, osmotic compressibility and thermoelectric power. Polymer *21*, 274–278.

Matter, Volume *5*

Supplemental information

Dynamically modulated gating process of nanoporous membrane at sub-2-nm speed

Yahong Zhou, Junran Hao, Jiajia Zhou, Jingwen Liao, Yan Wei, Xiachao Chen, Chengyun Ning, Xuliang Deng, and Lei Jiang

Supplemental Information

Dynamically Modulated Gating Process of Nanoporous Membrane at Sub-2 nm Speed

Yahong Zhou, Junran Hao, Jiajia Zhou, Jingwen Liao, Yan Wei, Xiachao Chen, Chengyun Ning, Xuliang Deng, and Lei Jiang

This file includes:

Section S1. Chemicals and characterization methods.

All chemicals of analytical grade were purchased from Aladdin Chem Co., Ltd. and used without further treatment if not specified otherwise. The AAO membranes with thickness of 60 μm were obtained from Hefei Pu-Yuan Nano Technology Ltd, which prior to use were rinsed and degreased ultrasonically in deionized water, ethanol and acetone, respectively. Doubly distilled water (> 1.82 MΩ cm, MilliQ system) was used. Field emission scanning electron microscopy (FE-SEM, ZEISS Ultra 55, Germany) and transmission electron microscopy (TEM, JEOL JEM-2100, Japan) were employed to examine the results at various dimensions. Energy-dispersive x-ray (EDX, Oxford INCA, Britain) technique was utilized to analyze the chemical composition of selected region on as-obtained products.

Section S2. Preparation route of CPNMs.

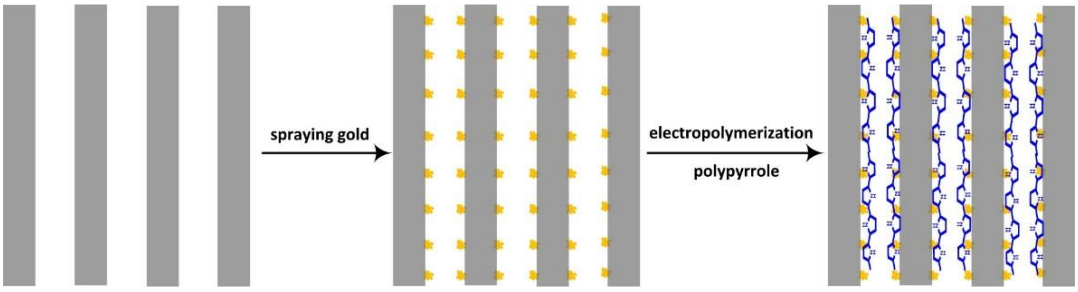

Fig. S1. Schematic illustration of preparing CPNMs in AAO membrane. Gold particles were sputtered on the inner surface of nanopores through AAO membrane. Py monomers migrated into nanopores and were electropolymerized to PPy, which partly filled the nanopores. In this way, CPNM embedded in AAO membrane were obtained.

The CPNM was prepared by electrochemical polymerization methods. The small electrochemical cell included a double-pass AAO membrane (effective area of 110 mm2) with gold sputtering (working electrode), copper sheet (counter electrode), saturated calomel electrode (SCE) (reference electrode) and an electrolyte. The CPNM were obtained through cyclic voltammetry (0.80 - 0.85 V, 10 mV/S and 10 scanning cycles) at room temperature with the electrolyte which is a 5 mM β-naphthalenesulfonic acid (NSA) solution containing 50 mM pyrrole (Py) under the control of electrochemical station, and dried in a vacuum atmosphere.

Section S3. FE-SEM images of AAO membrane and CPNM.

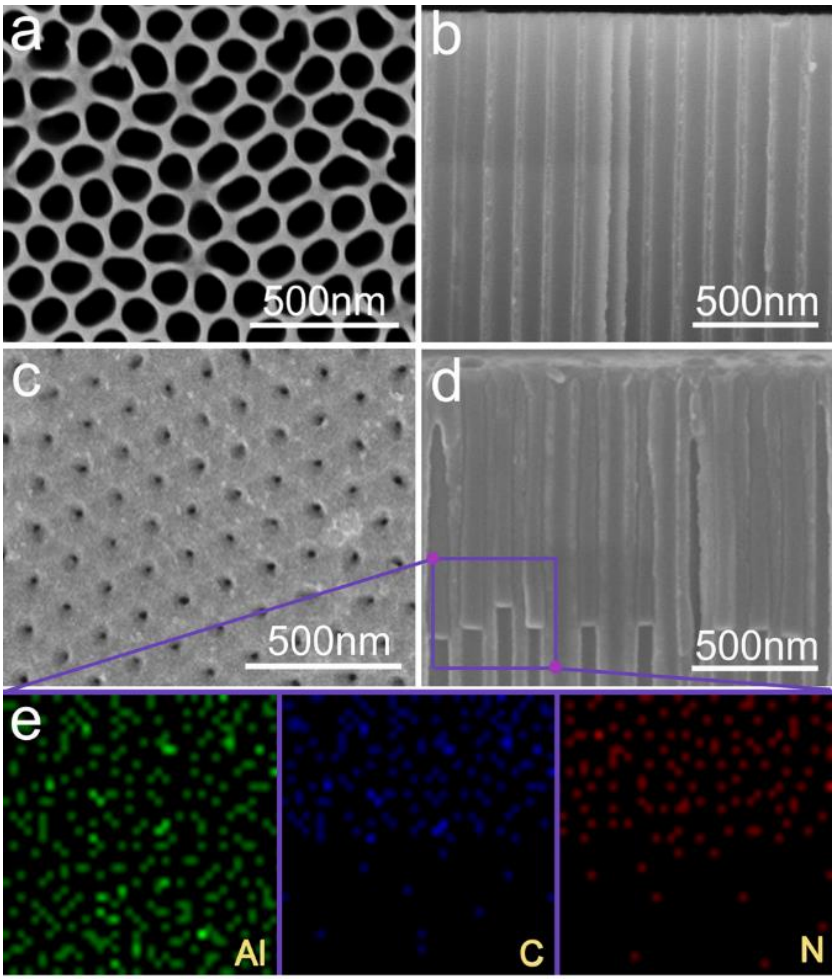

Fig. S2. FE-SEM images of AAO membrane and CPNM. **a**-**d**) FE-SEM images of top view and cross-sectional view of AAO (**a** and **c**) and CPNM (**b** and **d**) obtained by cyclic voltammetry of 10 cycles. **e**) EDX element distribution patterns of selected region.

As illustrated in Figure S2a and S2b, AAO membrane possessed a high density of relatively uniform nanochannel with about 100 nm in diameter and smooth inner wall. Among the 10 cycles (i.e., electropolymerization time) of cyclic voltammetry, the Py monomer was gradually electropolymerized to PPy along the inner wall of AAO nanopores. As a consequence, Figure S2c and S2d showed CPNM with 22.8 nm in inner diameter and 1 μm in length embedded into AAO nanopores. Moreover, EDX spectrum (Figure S2e) of selected region clearly indicated the geographical position and homogeneity of CPNM by the element (Al, C and N) distribution.

Section S4. Tunable diameters of CPNM based on polymerization times.

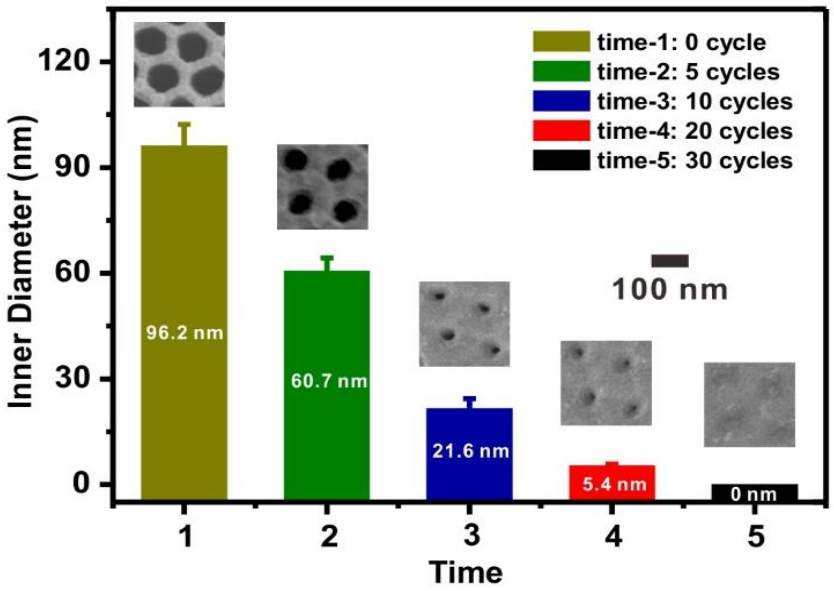

Fig. S3. The tunable inner diameters of CPNM based on polymerization times. The plot of inner diameters of CPNM vs polymerization time. Each data represents the average of at least five experiments.

Section S5. The relation of the wall thickness of CPNMs with cycle number of cyclic voltammetry.

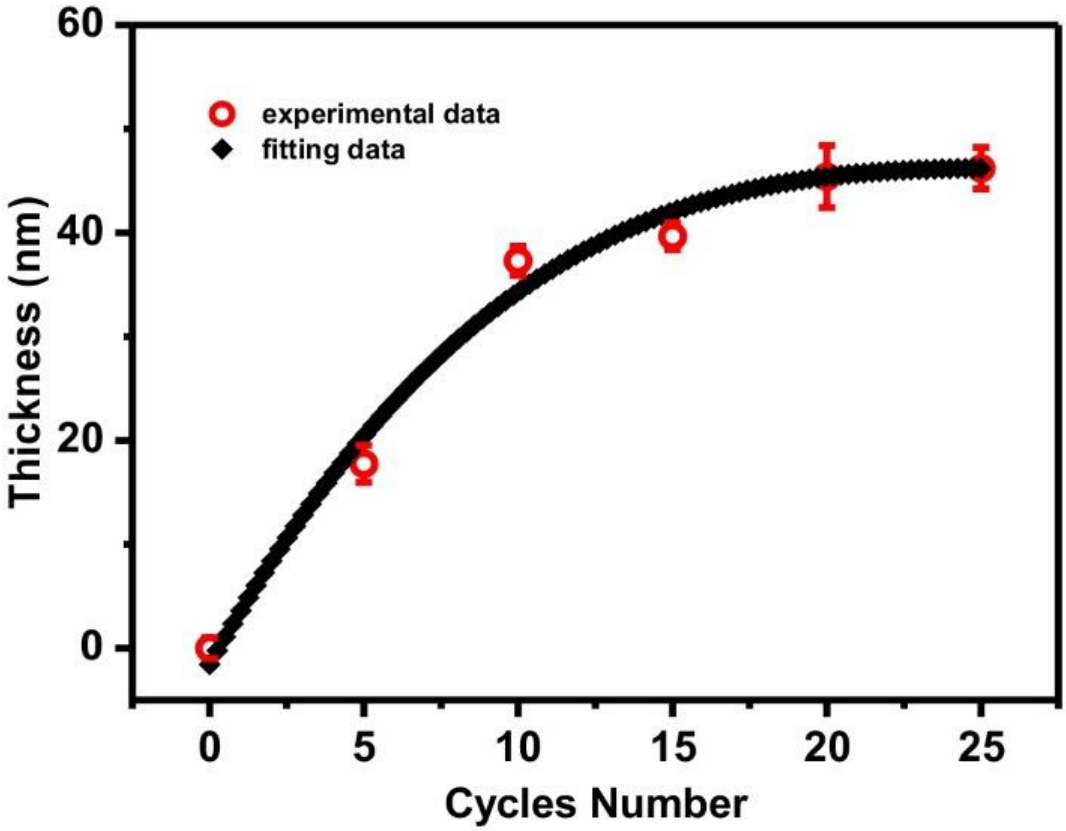

Fig. S4. The relation of the wall thickness of CPNMs with cycle number of cyclic voltammetry.

Section S6. *I-V* patterns of CPNMs obtained in various polymerization time and the plot of conductance *vs* inner diameters of CPNMs.

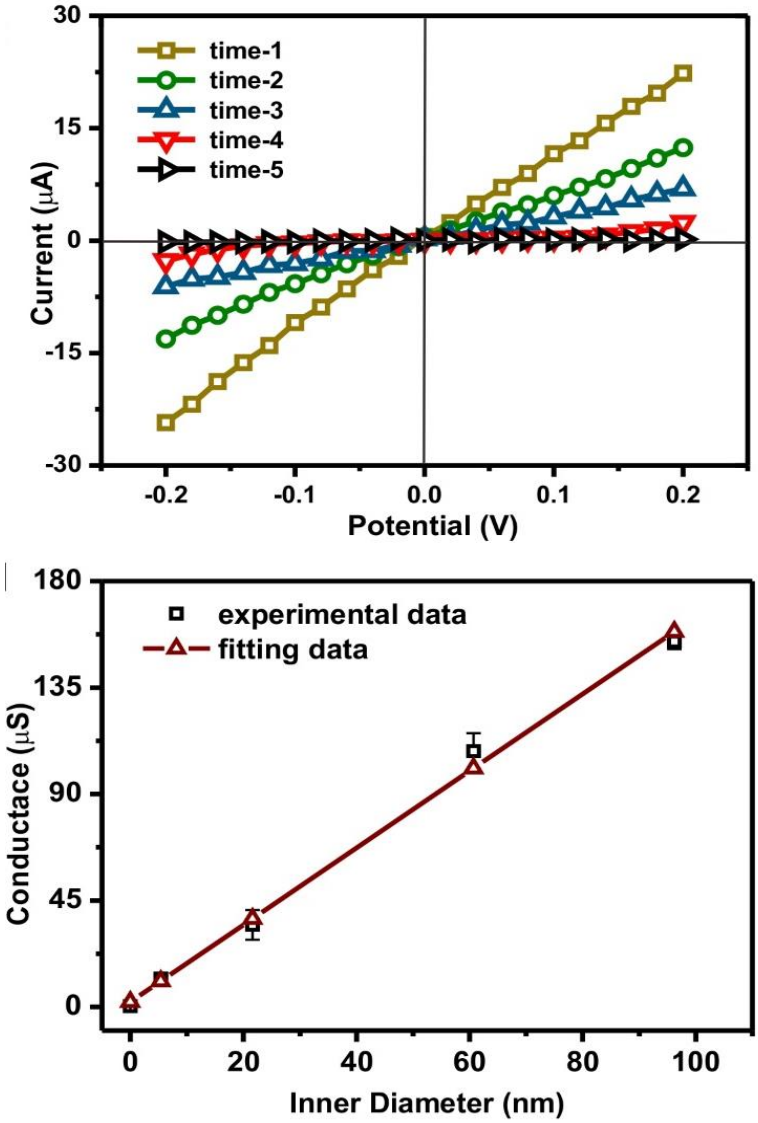

Fig. S5. *I-V* patterns of CPNMs obtained in various polymerization time (time 1-5 refer to 0, 5, 10, 20 and 30 cycles of cyclic voltammetry). Down: The plot of conductance *vs* inner diameters of CPNM and the straight line shows the linear fit of the experimental data.

We also studied the dependence of ion transport through CPNM on electropolymerization time realized by the cycle number of cyclic voltammetry. By adjusting the cycle number, we obtained a series of CPNM with inner diameters ranging from 0 nm to 96.2 nm and systematically investigated the current property of CPNM with different inner diameters. The relation of the wall thickness of CPNM obtained with different cycle number of cyclic voltammetry also indicated that the inner diameter of CPNM dropped down with electropolymerization time. The magnitude of ion current decreased to nearly 0 with the cycle number of cyclic voltammetry varying from 0 (i.e., AAO membrane) to 30 cycles. When the CPNM were formed by more than 30 cycles of cyclic voltammetry, the nanochannels with solid inner structure did not allow the

ion transport through them. That was to say, the ion transport could be modulated by electropolymerization time which affecting the channel space of CPNM. In addition, ion transport behavior through CPNM constructed in various diameters of AAO nanochannels was probed with the same electropolymerization time.

Section S7. *I-V* plots of CPNMs constructed in various diameters of AAO membranes.

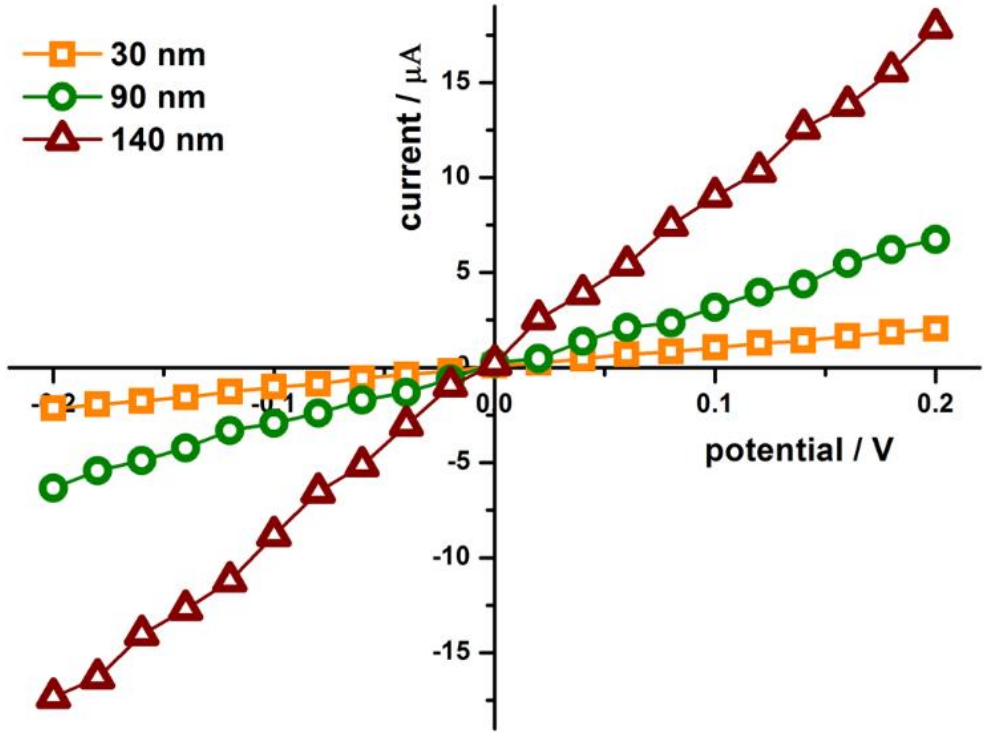

Fig. S6. *I-V* plots of CPNM constructed in various diameters of AAO nanochannels with the same electro-polymerization time (10 cycles).

The slopes of *I-V* patterns were increased with the diameters of AAO nanochannels. That was to say, larger inner diameter (or channel space) of CPNM obtained in larger diameter of AAO nanochannels offered larger conductance for ionic transport, which was accorded with Figure 4b. In addition, ion transport behavior through CPNM constructed in various diameters of AAO nanochannels was probed with the same electro-polymerization time (10 cycles).

Section S8. Cyclic voltammogram of CPNMs.

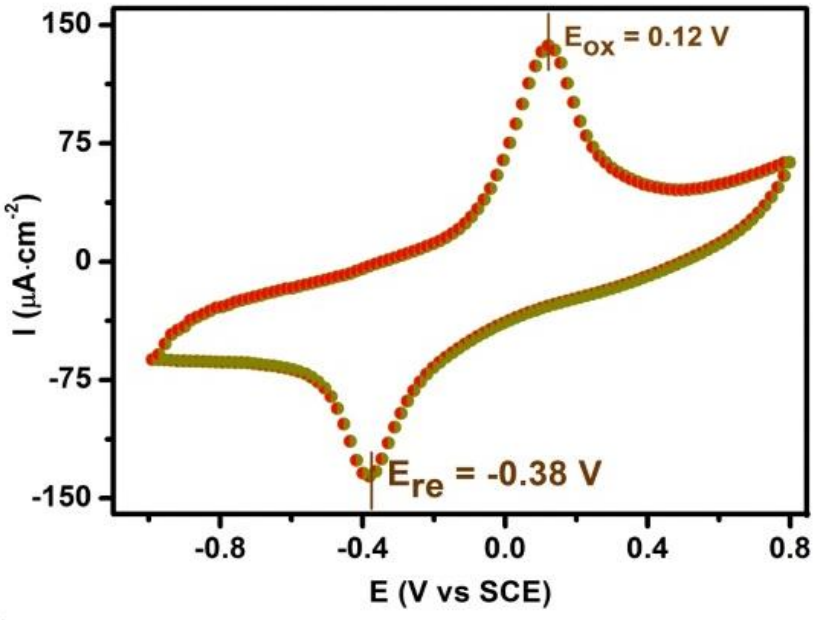

Fig. S7. Cyclic voltammogram of CPNMs. The oxidation peak is at 120 mV and reduction peak is at -380 mV.

To ascertain the redox-triggered potentials of CPNMs, cyclic voltammogram of CPNMs was recorded in pyrrole-free electrolyte including 5 mM β-naphthalenesulfonic acid (NSA). The oxidation peaks at 120 mV and reduction peaks at -380 mV showed the same absolute values of current (i.e., X axis of symmetry), indicating good redox reversibility of CPNMs, therefore providing an intelligent platform with the capacity for switching material.

Section S9. Verification of the open and close states of the CPNMs.

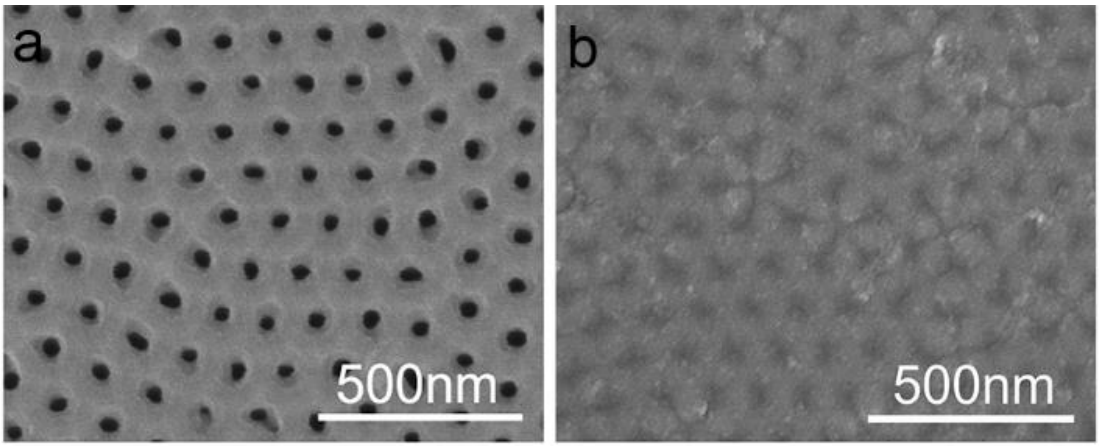

Fig. S8. Verification of the open and close states of the CPNMs. a, **b**), SEM images with open structures. The diameters of CPNMs were about 39.7 nm and 0 nm at the open and closed states. All data were obtained from the CPNMs that are fabricated by 10 cycles of cyclic voltammetry.

Section S10. Inner diameter distribution of CPNMs in various states.

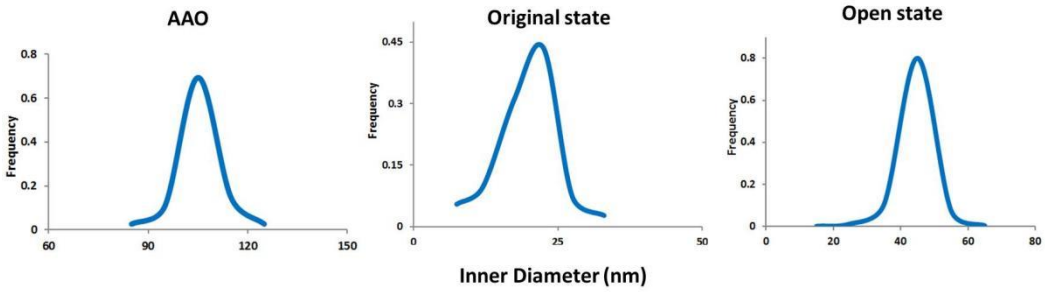

Fig. S9. Inner diameter distribution of CPNMs in various states.

The blank AAO membrane possessed pore size of about 100 nm. CPNMs embedded in AAO membrane showed inner diameters of approximately 22.8 and 45.1 nm in original and open (switch-on) states, respectively.

Section S11. Ionic transmembrane properties of CPNMs in different redox process.

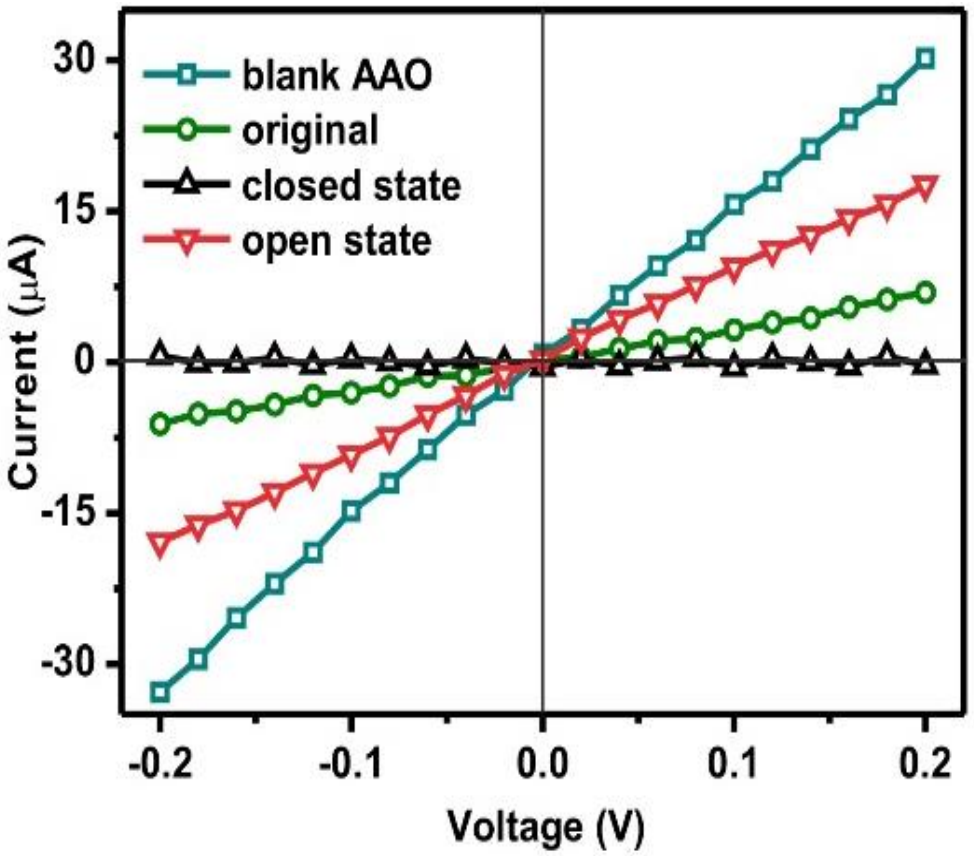

Fig. S10. Ionic conductance of CPNMs in redox process.

Section S12. Reversibility of the gating behavior.

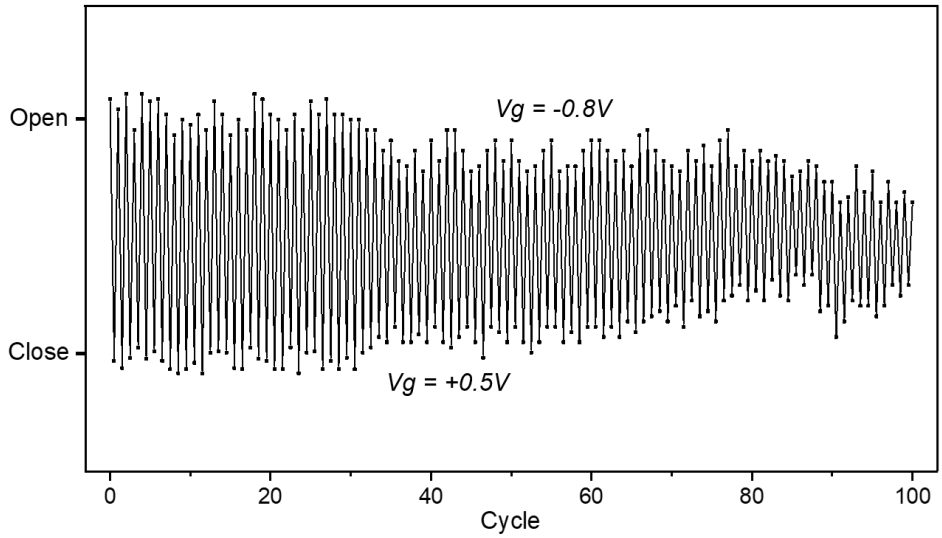

Fig. S11. The good reversibility of the redox gating process.

Section S13. Theory model of polymer film modulation speed between the charge and ions.

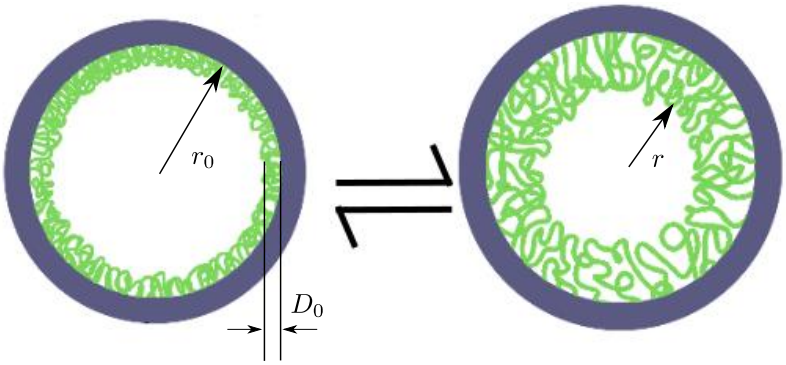

Fig. S12. Experimental setup: PPy network on the inner surface of AAO pores.

Pore Size Measurement

The experimental setup is shown in Fig. S8. The left figure shows the reduced state (or slightly oxidized state), corresponding to charge density on the PPy is small. In this case, the PPy network shrinks and the thickness of the PPy is small. The pore is at the open state. The thickness of the PPy is D_0 and the radius of the AAO pore is r_0=53 nm. The right figure shows the swollen state and corresponds to the oxidized and highly charged state. In this case, the inner radius r is small and the pore is closed.

Since the PPy network is confined at the inside of the AAO pores. Only in the radial direction the gel can expand. We assume that the area of the cross-section is swollen according to Eq. (4) in the manuscript.

$$\frac{\pi(r_0^2 - r^2)}{2\pi r_0 D_0} \sim \alpha^{1/2} \tag{1}$$

If we assume the charge ratio α depends on the time duration of the applied oxidization voltage. The resistance of a cylindrical pore is given by

$$R \propto \frac{L}{d^2} \propto \frac{L}{d_0^2 - k\alpha^{1/2}} \tag{2}$$

Here L is the length of the pore and d is the diameter. We also used Eq. (5) where k is a constant. The conductance of the whole system is given by

$$G = \frac{1}{R + R'} \propto \frac{1}{\frac{L}{d_0^2 - k\alpha^{1/2}} + R'} \tag{3}$$

where R' is the resistance from other parts in the system. A fit to the measurement value is shown in Fig. S12.

Fit (oxidized)

$$G = \frac{0.105869}{\frac{1}{40 * 40 - 565.7 * T^{1/2}} + 0.00046} \tag{4}$$

Here the unit of T is min.

Section S14. Conductance of theoretical and experimental data.

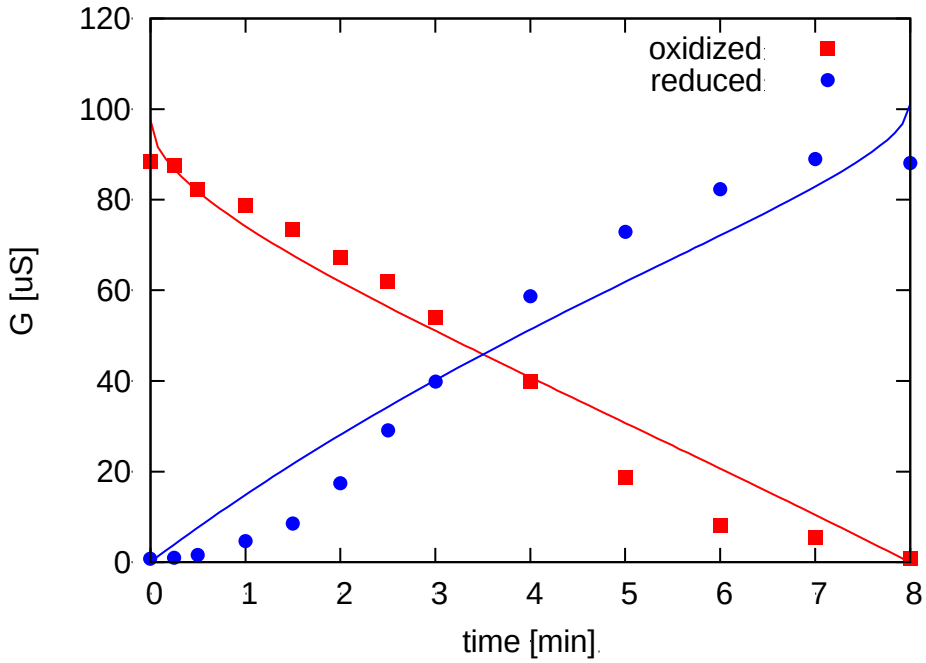

Fig. S13. The theoretical conductance fitting with the experimental data.

Section S15. The electrolyte effect on the conducting polymer nanoporous membrane.

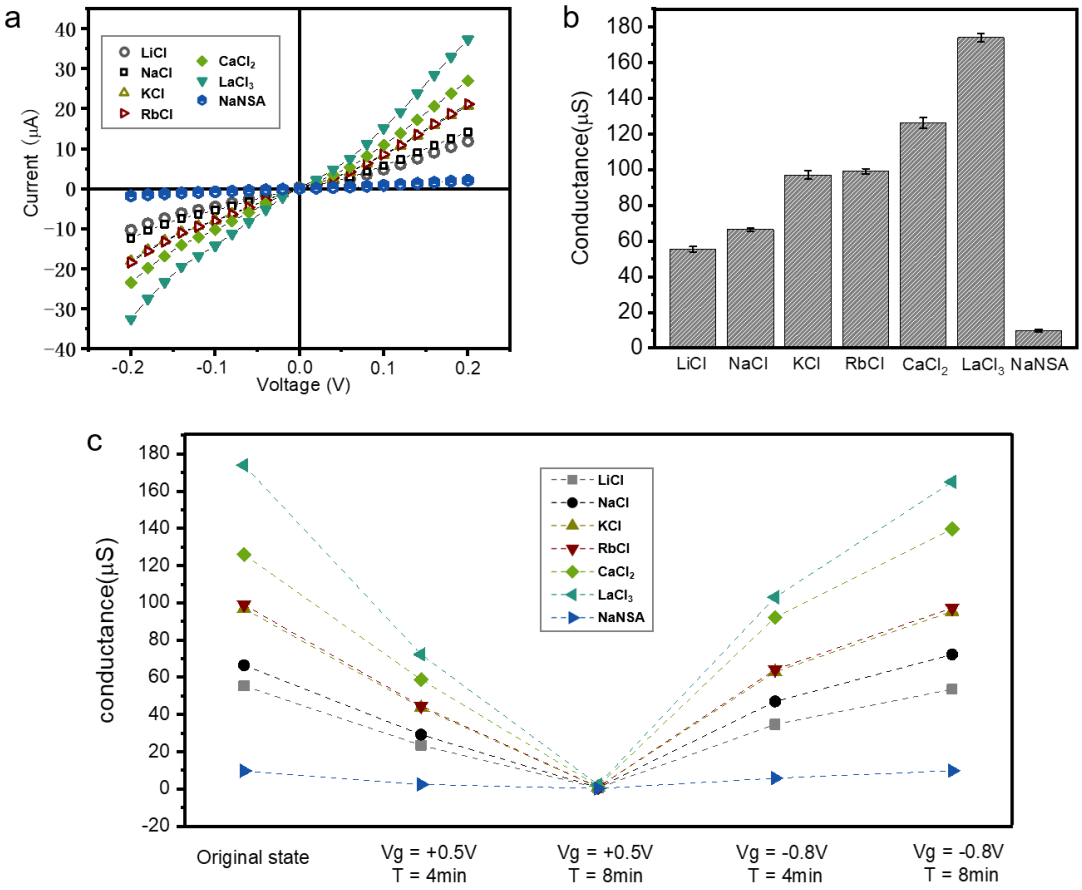

Fig. S14. The electrolyte effect on the conducting polymer nanoporous membrane. Ion current **(a)** and ion conductance **(b)** of the membrane under different types of electrolytes. **(c)** The conductance variation while the membrane is applied with redox potential under different electrolytes.

Section S16. The temperature-dependent current response of the membrane under open/close state.

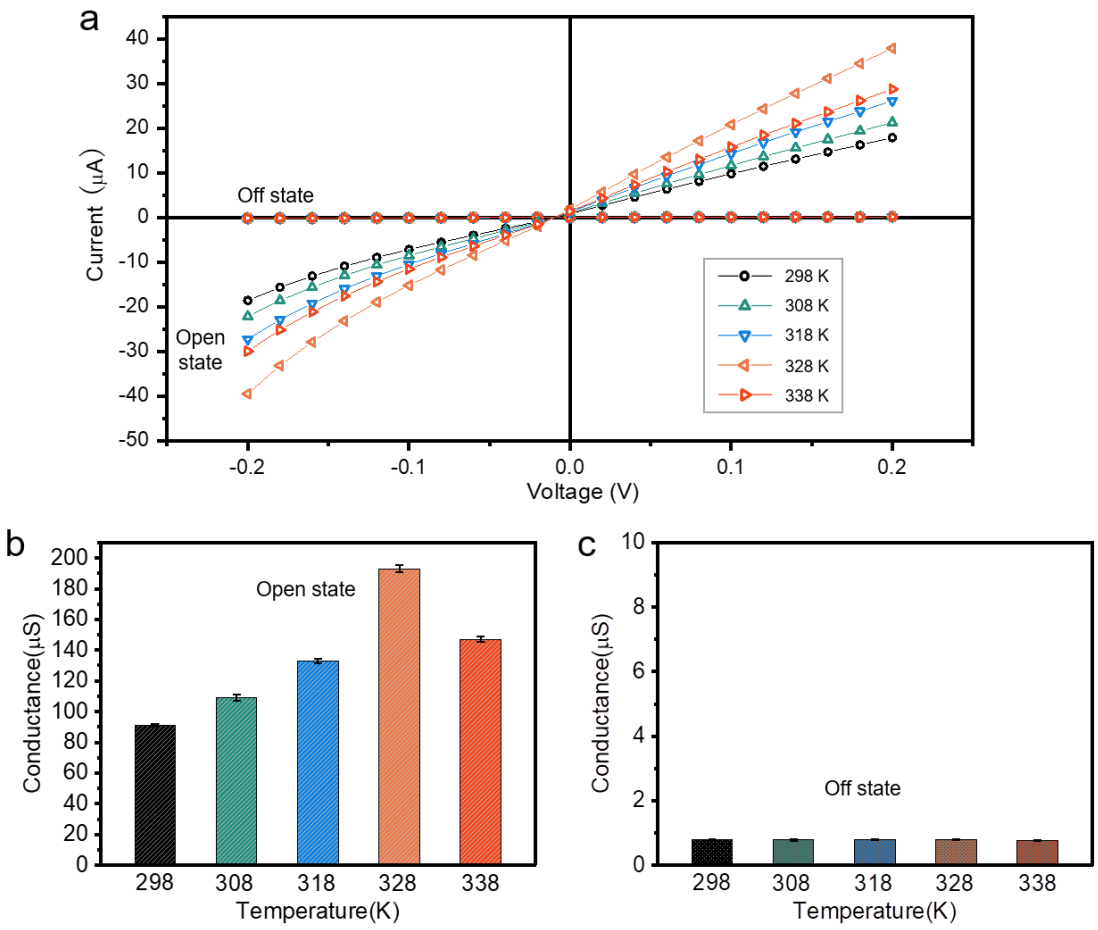

Fig. S15. The temperature-dependent current response of the membrane under open/off state. (a) Ion current of the membrane under different temperature. Ion conductance variation with the changing temperature at open state **(b)** and off state **(c).**

Section S17. The electrolyte effect on the conducting polymer nanoporous membrane.

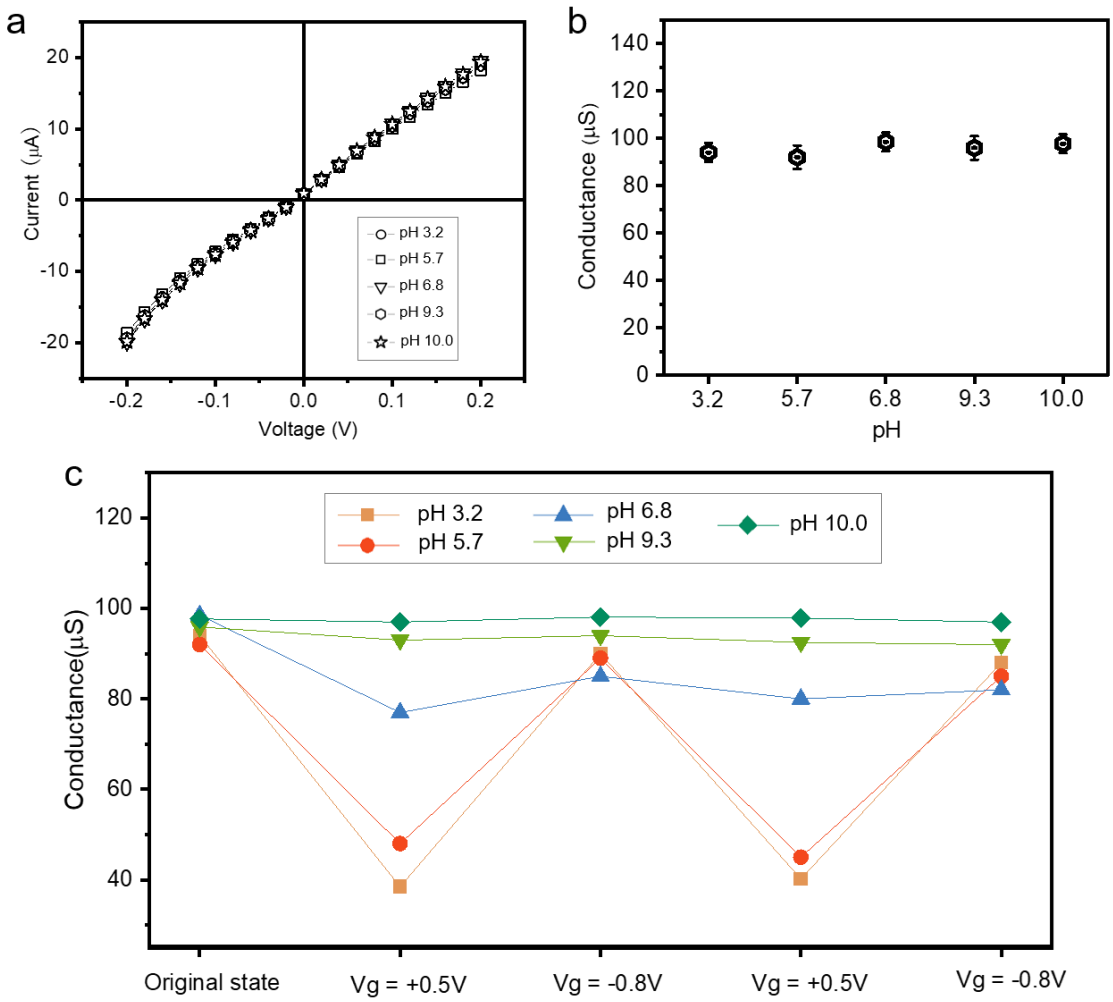

Fig. S16. The pH effect on the conducting polymer nanoporous membrane. The ion transmembrane current **(a)** and conductance **(b)** of the membrane under different pH value. **(c)** The conductance variation while the membrane is applied with redox potential under different pH.